IDENTIFICATION OF TRANSIENT AXIAL VIBRATION ON DOUBLE-SUCTION PUMPS DURING PARTIAL FLOW OPERATION

M.R.Hodkiewicz and J.Pan

School of Mechanical Engineering,

The University of Western Australia, Crawley WA 6009

The impeller in double-suction pumps is hydraulically balanced in the axial direction due to symmetry in the flow entering the two opposing suction eyes. While an assumption of axial balance is valid at design flow, process plant experience has shown that partial flow operation can result in dynamic axial displacement of the impeller causing mechanical seal and bearing failures. This paper investigates the effect of flow reduction on the axial vibration response of three sets of double-suction pumps and identifies transient axial vibration at partial flow using Short Time Fourier and Discrete Wavelet Transform techniques.

1. INTRODUCTION

Centrifugal pumps are simple mechanical devices, consisting of a rotating assembly contained within a housing. The rotating assembly includes an impeller mounted on a shaft that is supported by rolling element bearings. The impeller is usually driven by an electric motor attached to the shaft by a coupling. Fluid is retained within the pump by a mechanical seal or packing arrangement. The number and configuration of the impellers and the design of the casing determine the pump style.

This paper examines single-stage, horizontal split-case, double-suction impeller, volute pumps driven by fixed speed induction motors. A typical design is shown in Figure 1. Flow enters perpendicular to the plane of the drawing and is split into two annular suction chambers that turn and diffuse before entering the impeller through the opposing entrances. The flow fields from the two suction eyes are joined mid-way through the impeller vane passage and discharge into a common volute. When the impeller is centred in the casing and operated at the best efficiency point, the hydraulic forces acting on each side of the impeller are balanced.

Changes to the impeller flow field resulting from partial flow conditions include separation, secondary flows, stall, and recirculation [1-9]. The vibration of the pump was measured as the flow rate (Q) was reduced from the best efficiency point of operation (Q_{BEP}). Measurements indicate that loss of hydraulic balance and axial motion may be due to changes to the flow patterns that affect the forces acting on the impeller in double-suction pumps. It is postulated that this change can be detected as axial vibration on the bearing housing of the pump.

There has been limited published experimental work on the loss of axial hydraulic balance. One of the few experimental investigations of axial thrust of double-suction pumps used a load cell on the non-drive end of the shaft to record static and dynamic thrust. There was no change in the steady axial thrust but the unsteady axial thrust increased as flow was reduced [10]. This is consistent with recent published axial vibration data showing an increase in the root mean square value (RMS) of the vibration time signal in both axial and horizontal orientation as flow is reduced [11]. Published work on double-suction pumps in process plants has identified significant axial displacement of the pump shaft and associated damage to components due to partial flow operation [12, 13]. Mechanical seals will leak if the gap separating the rotating and stationary surfaces is compromised by axial displacements of the impeller. There is no widely accepted method of monitoring these pumps to identify and prevent damage during partial flow operation. This work investigates the response of three different double-suction pump designs to partial flow and examines the similarities and differences in response at identical operating points. The importance of signal processing technique is illustrated as conventional techniques fail to provide a complete picture of the non-stationary nature of the pump response as partial flow conditions develop.

2. DATA COLLECTION

Three separate water distribution pump installations (A, B & C) were tested. At each facility four pumps are installed in parallel with a common suction and discharge header. All pumps are split-case, double-suction, single-stage pumps driven by four-pole motors. Size and operational details of each set are shown in Table 1. At the time of data collection, the 'A' set of four pumps was a new installation; sets 'B' and 'C' had 30 months and 18 months continuous operation respectively. Vibration and performance data was collected on each of the pumps at discrete operating points over a range of flows for 0.40 to 1.20 Q/Q_{BEP} by adjusting the position of a valve on the discharge line of each pump and running multiple pumps in parallel. At each operating point 150 seconds of

vibration data was digitally recorded from accelerometers stud mounted on the non-drive end bearing in the horizontal and axial orientations. Performance data including flow, pressure and pump efficiency was measured using a Yatesmeter. Details of the data collection and Yatesmeter operation are described in [11].

	Set A	Set B	Set C
Installation date	2000	1997	2000
Number of pumps	4	4	4
Impeller diameter	453 mm	498 mm	402 mm
Duty Flow	405 l/s	463 l/s	270 l/s
Duty Head	60 m	71 m	45 m
Duty Power	264 kW	364 kW	133 kW
Flow at BEP	347 l/s	450 l/s	235 l/s
Maximum Efficiency	90.2%	88.5%	89.5%
Number of vanes	7	6	7
Volute style	Single	Double	Single
Pump bearings	2 x radial	Radial & thrust	2 x radial

Table 1: Pump Technical Information for Sets 'A', 'B' and 'C'.

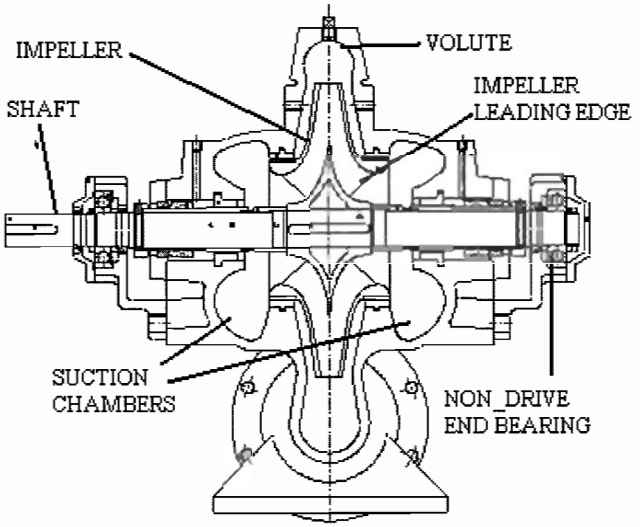

Figure 1: Schematic view of the double-suction pump.

3. DATA PROCESSING

Data from the digital tape recorder was sampled at 2 kHz using a National Instrument PCI-4552 board providing four channels of simultaneously sampled 16 bit data. Subsequent signal processing used LabView and Matlab software. All data presented in this report is in units of acceleration (m/s2). The effect of flow changes on conventional time and frequency representations of the vibration signal is described in [11]. This paper extends previous work by including an additional two pump sets, examining the non-stationary nature of the signal at partial flow and using Short Time Fourier Transform (STFT) techniques to identify transient events.

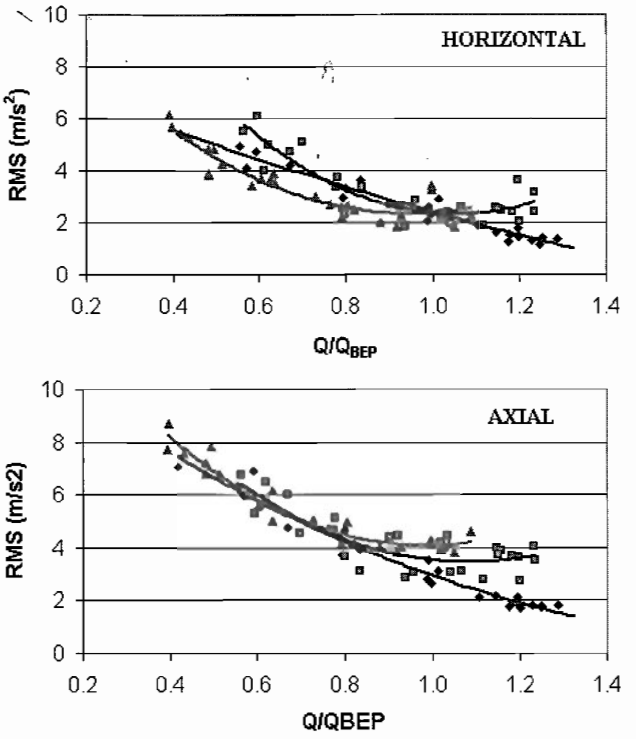

Figure 2: Comparison of RMS value of acceleration at the non-drive end bearing housing orientated axially and horizontally against Q/QBEP ratio. ◆ Set A, ■ Set B, ▲ Set C.

4. RESULTS

4.1 Statistical variables

Figure 2 shows the root-mean-square (r.m.s.) ψ_x of the time domain vibration signal (x_i) as a function of Q/Q_{BEP}. This is defined mathematically as

$$\psi_x = \sqrt{\psi_x^2} = \sqrt{\frac{1}{n}\sum_{i=1}^{n} x_i^2} \qquad (1)$$

where n is the number of samples x_i in the signal.

Each trend line represents the average for each set of four pumps (A, B and C). There is obvious correlation in the general trends of the graphs with an increase in RMS value of the signal as Q/Q_{BEP} is reduced. The response measured by the axially orientated accelerometer on these pumps is greater than that from the horizontal. The magnitude of the axial response doubles as flow is reduced from 1.0 to 0.5 Q/Q_{BEP}.

4.2 Stationarity

Signal characteristics such as stationarity, normality and the presence of periodic components determine the appropriate methods for signal analysis. Stationarity for an individual time history generally means that the statistical properties (mean, mean-square and variance) computed over short time intervals do not vary significantly due to statistical sampling variations from one interval to the next. Stationarity is important as the procedures for analysing non-stationary and transient data are

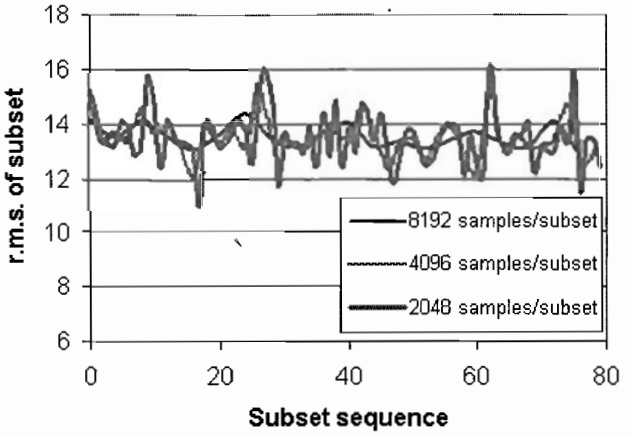

Figure 3: The effect of subset length (N) selection on the appearance of a plot of root mean square value of the subset along the length of the signal (n).

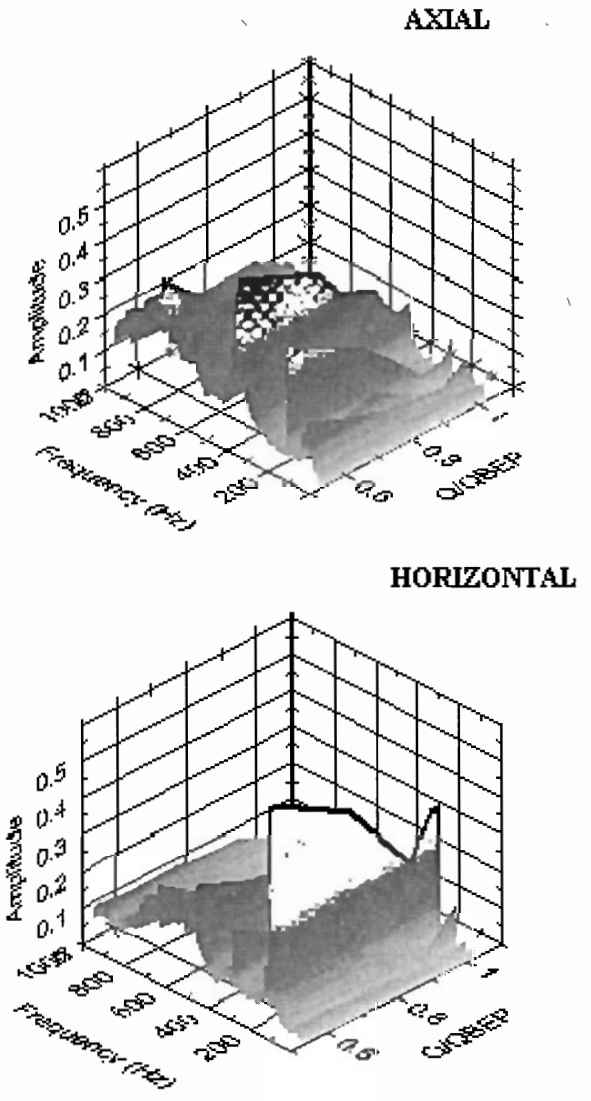

Figure 4: Waterfall plot of averaged Fourier spectra of axial and horizontal accelerations against Q/QBEP for Pump Set A3.

more complicated than for stationary data [14].

There are different procedures available for examining stationarity but no definitive process. A normalised r.m.s error calculation and visual examination of the change in mean square value of subsets of the signal with time were used to assess stationarity. The mean square value of a signal subset of length N where $N<<n$ is

$$\hat{\psi}_x^2 = \frac{1}{N}\sum_{i=1}^{N} x_i^2 \qquad (2)$$

Visual examination of the change in $\hat{\psi}_x^2$ along the length of a signal provides only a qualitative assessment of the non-stationary effects. Comparisons between different signals are complicated due to the increased variance of the signal with increasing mean square values. However it is a useful method to assess the effect of signal processing parameters. The effect of subset length selection on a plot of the mean square value of the signal with time is shown in Figure 3. A subset length of 8192 samples produces a pseudo-stationary signal with little variation from the mean along the length of the entire signal. This set length is used for averaged Fourier analysis giving a frequency resolution of 0.25 Hz. Subset lengths of 4096 samples retain the non-stationary nature over the length of the signal but are approximately stationary within each subset. For STFT, sample set lengths of both 4096 and 1024 samples are used and the differences in the resulting Spectrogram plots examined.

4.3 Averaged Fourier transform

The Fast Fourier Transform (FFT) is commonly applied to the analysis of stationary signals from rotating equipment. In volute-style pumps there is usually a strong periodic component called vane pass frequency fv caused by the passage of each impeller blade past the tongue(s) in the volute. This appears as a sharp peak in a plot of the FFT amplitude spectrum and often represents the largest single contributor to an averaged spectrum. Averaged amplitude spectra are produced by windowing overlapped samples sub-sets of length 2N, applying a Fourier transform, and averaging the resulting arrays over m sets $\overline{X_k}\big|_m$. Examples of the effect of flow rate on amplitude spectra to 1kHz for a single pump measured with axial and horizontally oriented accelerometers are shown in Figure 4. The dominant frequency below 200 Hz corresponds to a sharp narrowband peak at the vane pass frequency, this appears on all the pumps. Above 200 Hz there are broadband "haystack" responses especially on the axial accelerometer, the frequency location and width of the bands depends on the individual pump.

A simple method of comparing the contribution of the transient and noise components for signals collected at various Q/QBEP operating points is developed below. From Parseval's theorem the mean square value of a time signal of length n is the same magnitude as the mean square value of the signal after Fourier transformation [14]. When the frequency based mean square calculation on a signal of length n is replaced by a calculation from the average of a number of frequency calculations based on a subset size N where N<<n, a difference δ occurs between the two magnitudes. The

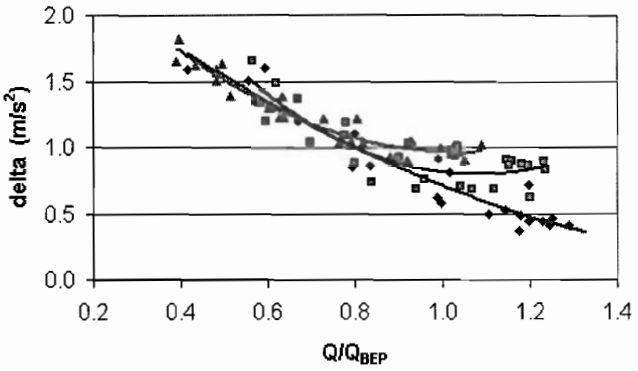

Figure 5: Comparison of difference d between calculations of signal magnitude in the time and frequency domain plotted against Q/QBEP ratio for the accelerometer on the non-drive end bearing housing orientated axially.
◆ Set A, ■ Set B, ▲ Set C

calculation is given in Equation (3).

$$\delta = \left[\psi_x^2 - \tfrac{1}{2} \sum_k \bar{X}_k^2 \right] \tag{3}$$

The magnitude of δ is zero for sinusoidal signals without noise contributions. The value of δ increases when noise and transient contributions are present A plot of δ for all the pumps against Q/Q_{BEP} in Figure 5 shows increasing divergence between the two lines as flow is reduced. This divergence represents the contribution of noise and non-periodic effects at partial flow that are retained in the RMS calculation but removed by the averaged Fourier process.

The magnitude of δ should be close to zero. A plot of δ for all the pumps against Q/Q_{BEP} in Figure 5 shows increasing divergence between the two lines as flow is reduced. This divergence represents the contribution of noise and non-periodic effects at partial flow that are retained in the RMS calculation but removed by the averaged Fourier process.

4.4 Discrete Wavelet process for filtered frequency bands

Preservation of the transient and noise contributions is achieved by analysis of the signal in the time domain. In order to understand how the energy distribution within the signal changes with flow conditions a method that filters the signal without loss or distortion is required. This can be achieved by decomposition of the signal into a series of dyadic frequency bands using a discrete wavelet transform process [15]. A procedure for decomposition and reconstruction of the signal into frequency bands (detail levels) using the Daubechies 8 wavelet is described in a previous paper [16]. The effect of flow rate on the change in RMS value of each of these bands by pump set is illustrated for the axial accelerometer signal in Figure 6. There is good correlation within each pump set for the higher frequency bands down to and including the Detail Level 5 (42-85 Hz) band and clear correlation between increasing RMS value in the band and decreasing flow rate. The magnitude within the lower frequency bands is small due in part to the choice of acceleration for the display units on the graphs.

Of primary interest for this work is the effect of partial flow on the frequency response below 200 Hz where rhe

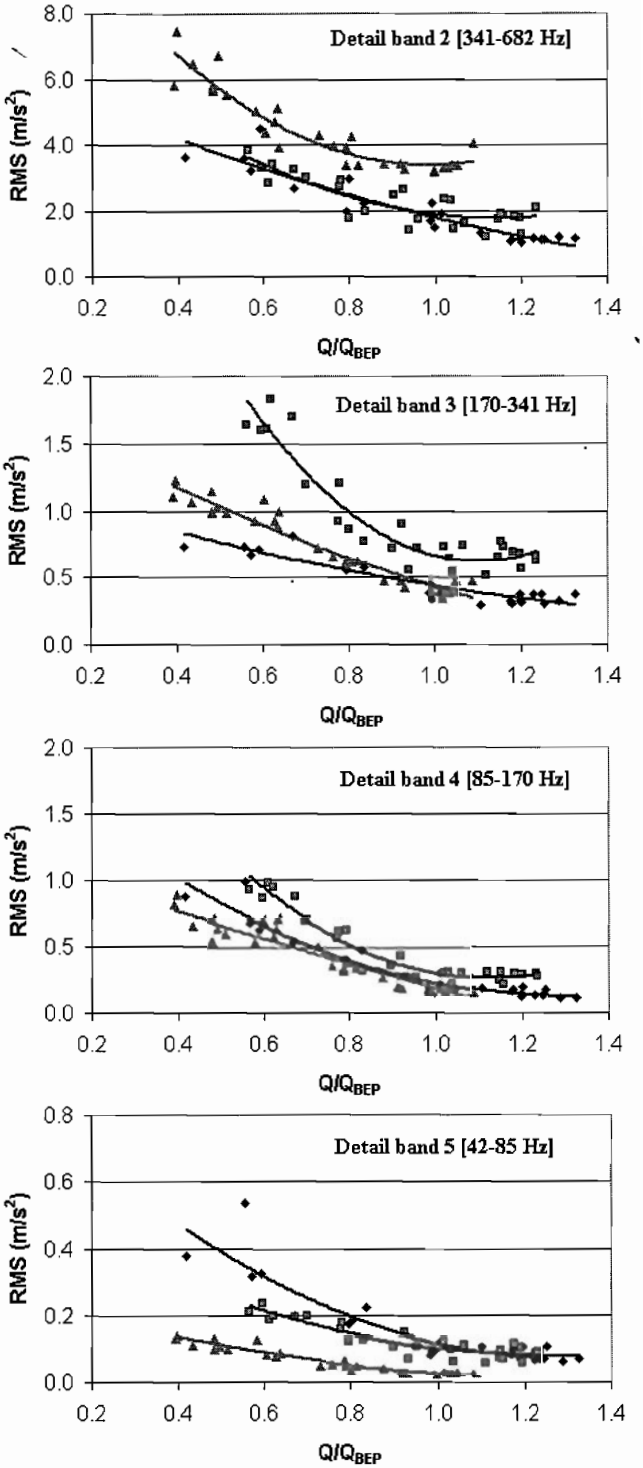

Figure 6: RMS value (m/s2) for the axial accelerometer signal separated into dyadic frequency bands plotted against Q/QBEP ratio. ◆ Set A, ■ Set B, ▲ Set C

majority of the vibration energy is concentrated. In order to examine the frequency and nature of the contributions from flow excitation and structural modes, tools such as the STFT or Continuous Wavelet transformation (CWT) techniques are required.

4.5 Short-time Fourier spectrograms

The STFT performs a Fourier transform on a single windowed data set of length 2N. The process is repeated for each data set as the window moves along the time signal in overlapping sections. The results are displayed as a Spectrogram plot with axes frequency, time and amplitude. Use of the STFT is optimized by the correct selection of window length for the frequency band of interest. The minimum window length must be greater than the largest potential frequency of interest. For these pumps this is 2 Hz or a window length of 68 samples. A larger window value will increase frequency resolution at the expense of time localization.

Figure 7 shows four spectrogram plots for the Pump A3 with a frequency resolution of 0.5Hz. Top plots are for the axial and horizontal accelerometers at 1.0 Q/Q_{BEP} and lower plots are at partial flow (0.4 Q/Q_{BEP}). This set of graphs illustrates the negligible axial and horizontal vibration measurements at 1.0 Q/Q_{BEP}. Partial flow operation results in significant peaks of varying amplitude and frequency measured by the axial accelerometer. These peaks are not synchronous with the pump rotating speed (24.8 Hz). Changes to the horizontal accelerometer plot between 1.0 $Q/_{QBEP}$ and partial flow are confined to the region close to *fv* (175 Hz). Similar features appear in spectrograms for the other pumps, although the location and width of the frequency bands appearing at partial flow vary with each pump set.

Figure 8 shows spectrogram plots from the axial accelerometers for one pump from each of Set A, B and C, at partial flow close to 0.6 Q/Q_{BEP}. Only a single plot for the horizontal accelerometer is shown, as it is typical of the other sets. The frequency resolution is increased to 2 Hz to improve time localisation. The time span illustrated represents 40 seconds of pump operation. The amplitude within each window is normalized by the amplitude of the vane pass frequency band in the window to illustrate the magnitude of the transient vibration relative to vane pass magnitude. These graphs illustrate the presence of transient vibration measured by the axial accelerometer on all the pump sets. There are generally consistent patterns within each set of pumps but marked differences in the appearance and magnitude of transient events between the sets. Differences in design will contribute to this, Pumps A and C are single volute casings with radial bearings, Pump B has a double volute casing and both radial and thrust bearings. For the horizontal response, the effect of partial flow is to increase the magnitude of *fv* but not significantly increase frequencies below *fv*.

CWT maps of these signal were examined but the two dimensional presentation in black and white is not as visually

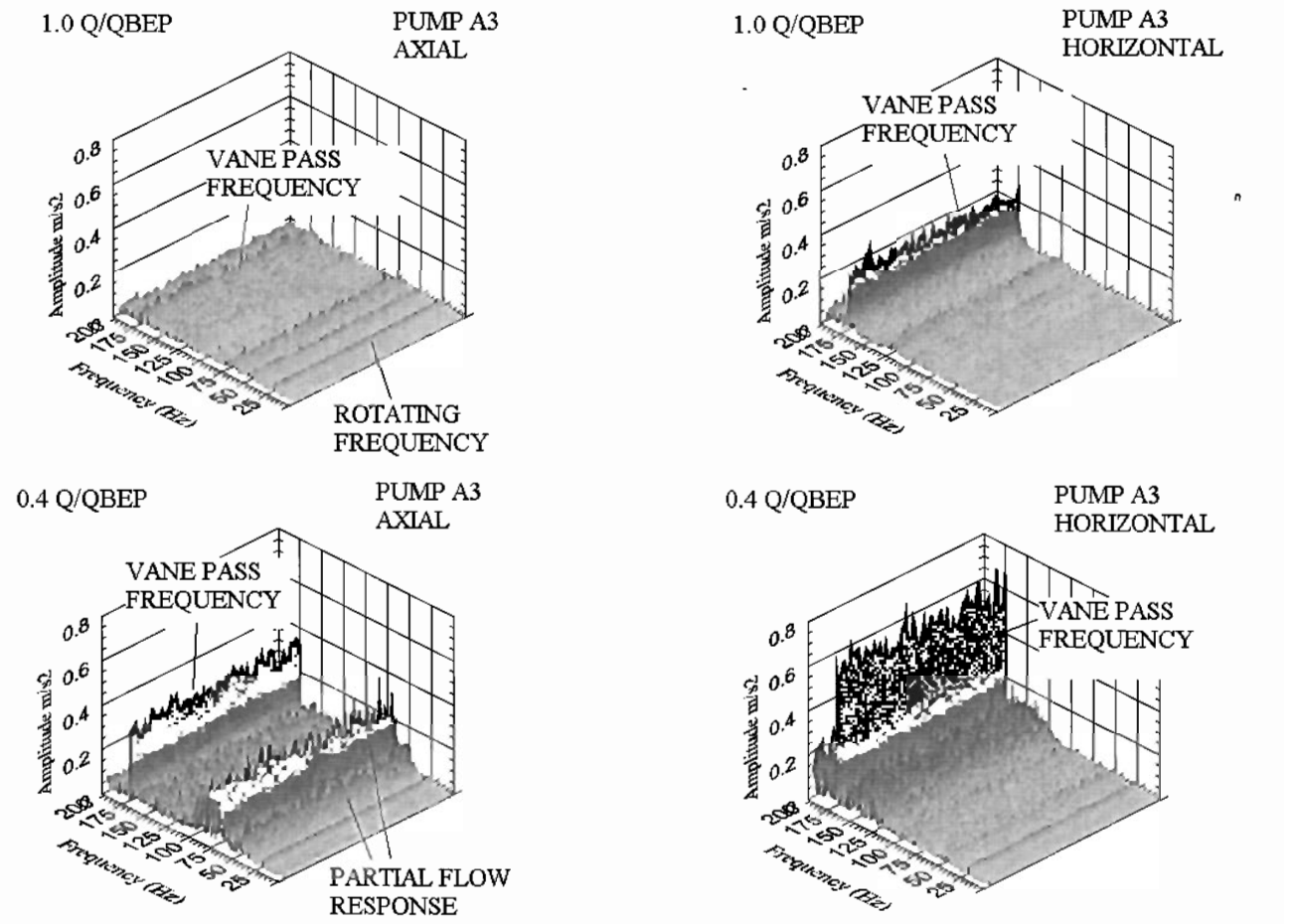

Figure 7: Spectrogram to 200 Hz comparing the axial and horizontal acceleration response at 1.0 Q/QBEP and 0.4 Q/QBEP for Pump A3. Frequency resolution is 0.5 Hz.

accessible as the three-dimensional Short-time Fourier spectrogram plots. Examples of CWT maps for these pumps are provided in [17].

4.6 Normalised RMS error

A normalised RMS error $\varepsilon\left[\hat{\psi}_x^2\right]$ is used to quantify the transient contributions to the signal below 170 Hz. This calculation quantifies deviation of the mean square value of a signal subset length 1024 samples from the average mean square value of the entire signal.

$$\varepsilon\left[\hat{\psi}_x^2\right] = \sqrt{\frac{E\left[\left(\hat{\psi}_x^2 - \psi_x^2\right)^2\right]}{\psi_x^4}} \qquad (4)$$

The signal below 170 Hz was created by summation of the appropriate detail and approximation frequency bands resulting from the discrete wavelet decomposition and reconstruction process. The results are shown in Figure 9 for each pump set plotted against Q/Q_{BEP}. There is obviously an increase in the normalised RMS error in this low frequency range of the signal as partial flow develops.

DISCUSSION AND CONCLUSIONS

The vibration measured axially on the non-drive end bearing housing increases as flow is reduced below QBEP. The vibration magnitude is calculated from the RMS values of the time signal. There is a difference between the RMS magnitude of the time signal and a calculation based on averaged frequency contributions. This difference increases as the flow is reduced and indicates that transient and noise events are being removed by the averaged Fourier technique.

Examination of the axial vibration signal from the non-drive end bearing of a double-suction pump using conventional fourier analysis shows an increase in amplitude of vane pass frequency and some broadband response at the higher frequencies. Averaged spectral analysis gives no indication of the high magnitude axial vibration below the vane pass frequency that develops at partial flow. This has been identified visually using short-time fourier techniques.

The STFT plots show that there are transient peak frequencies below 200 Hz. These peaks occur within frequency bands specific to the pump. The peak frequencies vary and are not synchronous with the rotating speed of the

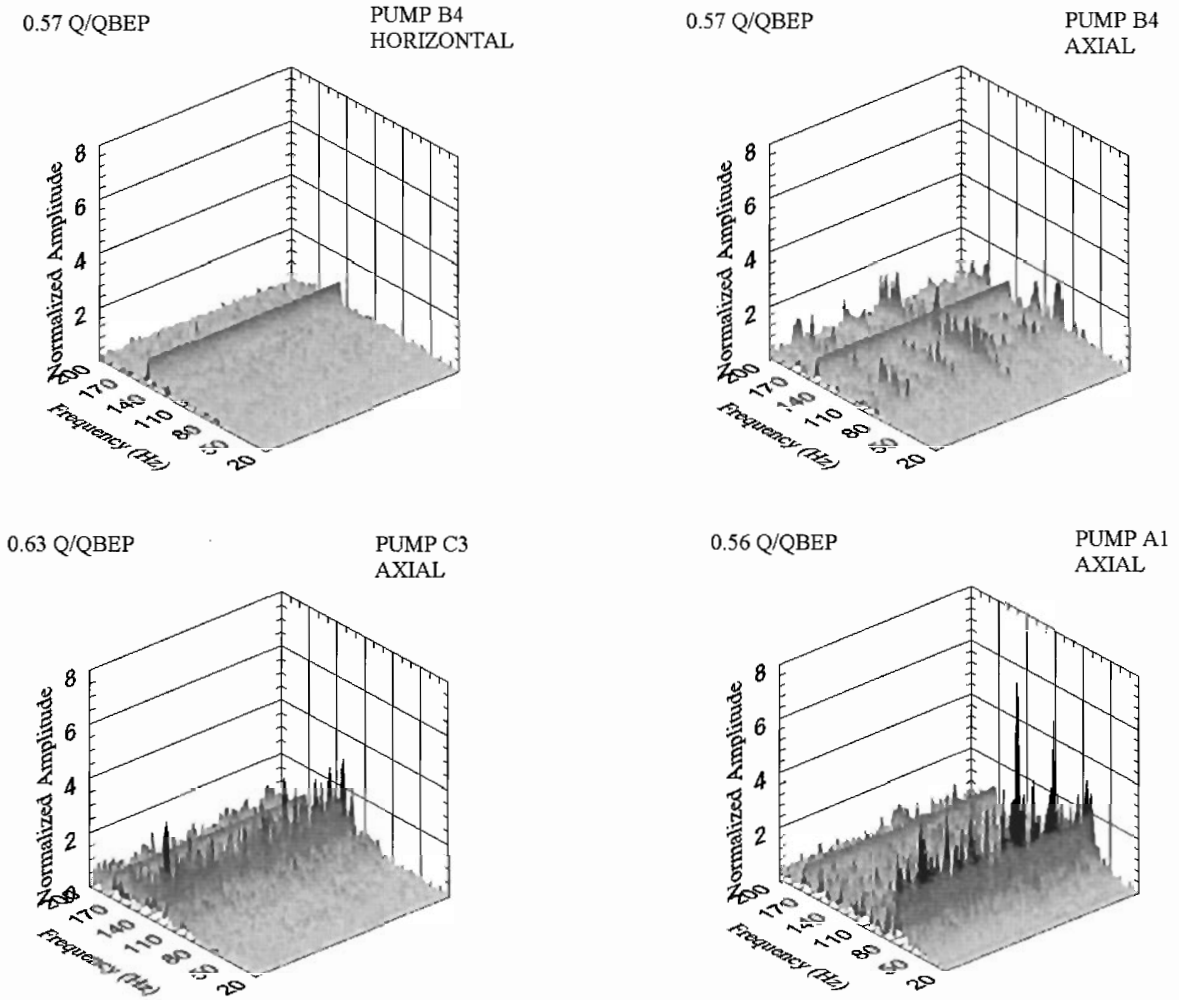

Figure 8: Spectrograms for the partial flow response of a pump from each set (A1, B4, C3) with the spectra normalised by the magnitude at the vane pass frequency.

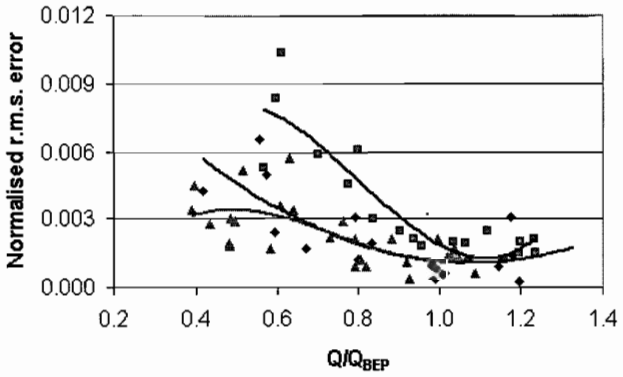

Figure 9: Normalised r.m.s/ error of the signal below 170 Hz for each pump set against Q/QBEP.
◆ Set A, ■ Set B, ▲ Set C

pump. The magnitude of the transient peaks below 200 Hz can exceed the vane pass contribution to the signal. The increased contribution from these transient events is quantified by calculation of the normalised RMS error of signal subsets; this increases as flow is moved away from QBEP.

Observations for the axial accelerometer response at partial flow operation can be summarized as follows

1. The vibration is a minimum close to Q_{BEP} and increases above and below this operating point
2. Transient events with frequencies below 200 Hz occur during partial flow operation.
3. The transient components are not related to the rotational frequency of the pump.
4. The transient events appear as regions of high magnitude localized in time.
5. The magnitude of transient events is equal to or exceeds the vane pass frequency magnitude.
6. The normalised random error of the signal subsets (below 170 Hz) from the mean increases as flow is reduced.
7. There is minor variation in the magnitude of the vane pass frequency with time at partial flow.
8. The frequency range in which low flow excitation response occurs is broadly consistent within a set of identical pumps, but varies between pump sets.

The measured axial vibration is affected by the unsteady axial thrust on the double-suction impeller at partial flow. There are two sources of axial thrust, the pressure on the impeller shroud surfaces and the change in axial momentum through the pump.

An unsteady net pressure difference between the external surfaces of the opposing impeller shrouds produces a net axial force. The magnitude of this force is determined by the integral of the pressure over the surface area of each shroud. Pressure is affected by the flow field within the shroud-casing space which is determined by the configuration and dimensions of the space, the entrance dimensions, circumferential and axial components of the fluid velocity leaving the impeller at the shroud surface, clearance and condition of the wear ring seals, and the surface conditions of the impeller and casing [18]. A loss in symmetry in the pressure distribution between the opposing shroud surfaces due to partial flow perturbations entering the shroud-casing spaces will create unsteady axial motion.

An asymmetric change in the magnitude of the axial component of momentum between the inlet and outlet of the impeller will produce axial thrust. Any loss of symmetry between the inlet velocity and discharge velocity in the two halves of the impeller due to unsteady entrance conditions and internal flow separation will result in an unsteady axial force.

There are no detailed published studies on the pressure or velocity distributions within a double-suction pump at partial flow or the relative effect of each of the axial thrust contributions to the overall axial thrust. The effect of partial flow operation on unsteady axial shaft displacement and its relationship with bearing housing axial vibration is the subject of continuing investigation.

ACKNOWLEDGEMENTS

The authors wish to thank the Systems Investigation Unit of the Water Corporation of Western Australia for the Yatesmeter performance data, Joanna Sikorska for assistance with the STFT program and Dr. Angus Tavner for reading the manuscript.

REFERENCES

1. Pedersen, N., P.S. Larsen, and C.B. Jacobsen, "Flow in a centrifugal pump impeller at design and off design conditions - Part 1: Particle image velocimetry (PIV) and Laser Doppler Velocimetry (LDV) measurements" *ASME Journal of Fluids Engineering* **125** 61-72 (2003)
2. Parrondo-Gayo, J.L., J. Gonzales-Perez, and J. Fernandez-Francos, "The effect of the operating point on the pressure fluctuations at the blade passage frequency in the volute of a centrifugal pump" *ASME Journal of Fluids Engineering* **124** 784-790 (2002)
3. Gonzalez, J., et al., "Numerical simulation of the dynamic effects due to impeller-volute interaction in a centrifugal pump" *ASME Journal of Fluids Engineering* **124** (June), 348-355 (2002)
4. Kaupert, K.A. and T. Staubli, "The unsteady pressure field in a high specific speed centrifugal pump impeller - Part 1: Influence of the volute" *ASME Journal of Fluids Engineering* **121** 621-626 (1999)
5. Kaupert, K.A. and T. Staubli, "The unsteady pressure field in a high specific speed centrifugal pump impeller - Part 2: Transient hysteresis in the characteristic" *ASME Journal of Fluids Engineering* **121** 627-632 (1999)
6. Liu, C.H., C. Vafidis, and J.H. Whitelaw, "Flow characteristics of a centrifugal pump" *ASME Journal of Fluids Engineering* **116** 303-309 (1994)
7. Choi, J.-S., D.K. McLaughlin, and D.E. Thompson, "Experiments on the unsteady flow field and noise generation in a centrifugal pump impeller" *Journal of Sound and Vibration* **263** 493-514 (2003)

8. Dong, R., S. Chu, and J. Katz, "Relationship between unsteady flow, pressure fluctuations and noise in a centrifugal pump - Part B: Effects of blade-tongue interactions" *ASME Journal of Fluids Engineering* **117** 30-35 (1995)
9. Kikuyama, K., et al. Unsteady pressure distributions on the impeller blades of a centrifugal pump-impeller operating off-design. *ASME Gas Turbine Conference and Exhibition*. Anaheim, California 1987.
10. Konno, D. Experimental research on axial thrust loads of double suction centrifugal pumps. *IMechE Seminar on Radial loads and axial thrusts in centrifugal pumps*. London 1986.
11. Hodkiewicz, M.R. and M.P. Norton, "The effect of change in flow rate on the vibration of double suction centrifugal pumps" *Proceedings of the Institute of Mechanical Engineers Part E: Process Mechanical Engineering* **216** 47-58 (2002)
12. Makay, E. and J.A. Barrett. Changes in hydraulic component geometries greatly increased power plant availability and reduced maintenance cost:case history. *Proceedings of 1st International Pump Users Symposium*. Texas 1984.
13. Stanmore, L.K. Field problems relating to high energy centrifugal pumps operating at part-load. *Part-load Pumping Operation, Control and Behaviour*. Edinburgh 1988.
14. Bendat, J.S. and A.G. Piersol, *Random Data - Analysis and Measurement Procedures*. Wiley Interscience (2000)
15. Strang, G. and T. Nguyen, *Wavelets and Filter Banks* (1997)
16. Hodkiewicz, M.R. and J. Pan. Identification of transient axial vibration on double-suction pumps during partial flow operation. Part I - Experimental and data processing methods. *10th Asia-Pacific Vibration Conference*. Gold Coast, Australia 2003.
17. Hodkiewicz, M.R. and J. Pan. Identification of transient axial vibration on double-suction pumps during partial flow operation. Part II - Transient axial response identification. *10th Asia-Pacific Vibration Conference*. Gold Coast, Australia 2003.
18. Kurokawa, J. and T. Toyokura. Study on axial thrust of radial flow turbomachinery. *Proceedings of the 2nd International JSME Symposium Fluid Machinery and Fluidics*. Keidanren Kaikan, Tokyo 1972.